Published in final edited form as:
FEBS Lett. 2008 November 12; 582(27): 3765–3770. doi:10.1016/j.febslet.2008.10.013.

Alternative splicing within the I–II loop controls surface expression of T-type $Ca_v3.1$ calcium channels

Aleksandr Shcheglovitov[1,*], **Iuliia Vitko**[1,*], **Isabelle Bidaud**[2,3,4,*], **Joel P. Baumgart**[5], **Manuel F. Navarro-Gonzalez**, **T. Hilton Grayson**, **Philippe Lory**[2,3,4], **Caryl E. Hill**[6], and **Edward Perez-Reyes**[1,5]

1*Department of Pharmacology, University of Virginia, Charlottesville, Virginia 22908, U.S.A.*

2*CNRS, UMR 5203, Institut de Génomique fonctionnelle, Montpellier, France*

3*INSERM, U661, Montpellier, France.*

4*Université Montpellier, 1 et 2, Montpellier, France.*

5*Neuroscience Graduate Program, University of Virginia, Charlottesville, Virginia 22908, U.S.A.*

6*Division of Neuroscience, John Curtin School of Medical Research, The Australian National University, Canberra, Australia.*

Abstract

Molecular diversity of T-type/Ca_v3 Ca^{2+} channels is created by expression of three genes and alternative splicing of those genes. Prompted by the important role of the I–II linker in gating and surface expression of Ca_v3 channels, we describe here the properties of a novel variant that partially deletes this loop. The variant is abundantly expressed in rat brain, even exceeding transcripts with the complete exon 8. Electrophysiological analysis of the Δ8b variant revealed enhanced current density compared to $Ca_v3.1a$, but similar gating. Luminometry experiments revealed an increase in the expression of Δ8b channels at the plasma membrane. We conclude that alternative splicing of Ca_v3 channels regulates surface expression and may underlie disease states in which T-channel current density is increased.

Introduction

Voltage-gated calcium channels, especially the $Ca_v3.1$ member of the T-type/Ca_v3 subfamily, are subject to extensive alternative splicing, which provides a substrate for phenotypic differences (reviewed in [1]). Although yet unexplored, it is tempting to postulate that splicing variations in regions that play a role in gating and surface expression of Ca_v3 channels, i.e., transmembrane domains I and II as well as the I–II loop [2–4], could result in significant changes in channel activity. While studying the mechanisms underlying rhythmical contractions of the juvenile rat basilar artery, we have identified specific roles and properties for both $Ca_v3.1$ T-type and $Ca_v1.2$ L-type calcium channels in controlling cerebrovascular tone

Address correspondence to either: Edward Perez-Reyes, Department of Pharmacology, University of Virginia, Charlottesville, VA 29908, U.S.A., E-mail: eperez@virginia.edu; or Caryl Hill, Division of Neuroscience, John Curtin School of Medical Research, The Australian National University, Canberra, Australia, E-mail: Caryl.Hill@anu.edu.au.
*A.S., I.V., and I.B. contributed equally to this work

[5]. However, such transient, low voltage activated channels would not be expected to remain open at the more depolarized potentials experienced by smooth muscle cells *in vivo* and hence may be considered to be unlikely candidates for control of cerebrovascular tone. It was therefore of considerable interest that alteration to sequences within transmembrane Domains I and II and the I–II linker of $Ca_v3.1$ channels could result in alterations to voltage gating [2–4]. As a result, we undertook cloning and sequencing of the $Ca_v3.1$ regions mentioned above to determine whether these arteries express undescribed splice variants of T-channels with properties matching those of smooth muscle cells. Through these studies, we discovered a novel splice variant in which the I–II loop lacked a 402 bp region encoding 134 amino acids [5]. Interestingly, deletion analyses performed in human $Ca_v3.1$ and $Ca_v3.2$ channels have shown that a comparable region of the I–II loop, named D3–5, plays a significant role in their expression at the plasma membrane [4,6]. The identification of a naturally occurring variant in a homologous region of $Ca_v3.1$ in the basilar artery, named Δ8b, promptly encouraged us to investigate its functional properties and also whether this variant is expressed within the brain, where T type channels play an important role in neuronal excitability and rhythmicity. Using a combination of techniques, including molecular biology, electrophysiology, and luminometry, these experiments provide a richer understanding of the structure and function of $Ca_v3.1$ channels, and, along with previous findings in $Ca_v3.2$, establish the intracellular I–II loop as an important governor of LVA calcium channel function and expression.

Materials and Methods

RNA isolation and RT-PCR

Basilar arteries and cerebral cortex were dissected from juvenile male Wistar rats aged 14–17 days, according to a protocol approved by the Animal Experimentation Ethics Committee of the Australian National University. The main basilar artery was separated from the smaller side branches (caudal cerebellar arteries) and mRNA extracted using RNeasy Mini Kits (QIAGEN, USA) and reverse transcribed to cDNA using oligo dT (500 ng/μL, Invitrogen) primers and Superscript II (200 U/μL, Invitrogen). cDNA was amplified using primers designed to span the I–II linker of $Ca_v3.1$ (forward; CAACACCACCTGTGTCAACTGGAA; reverse; AGCCTCCAGAAAGCCAGCACAGAA) as follows: 95° C for 120 s, 40 cycles of 95° C for 10 s, 66° C for 10 s, 72° C for 80 s, and a final cycle of 72° C for 5 min.

Total RNA was extracted from rat whole brain (6–8 week) or indicated sub-regions. cDNA was synthesized from 1 μg total RNA using random primers and the iScript select cDNA synthesis system following the manufacturer's recommendation (BioRad, Hercules, CA). Amplification reactions were performed in a Mastercycler gradient (Eppendorf, Westbury, NY, USA) using iTaq DNA polymerase (Bio-Rad). After a 150 s denaturation step, reactions were cycled 35 times using 25 s for denaturation (94° C) and annealing (70° C), and 80 s for extension (72° C). PCR products were cloned with the pCRII-TOPO kit (Invitrogen, Carlsbad, CA, USA). Products were run on 1–1.5% agarose gels, stained with ethidium bromide and image analysis conducted using either an Analytical Imaging Station software (Berthold Australia) or Adobe Photoshop. Preliminary experiments varying the number of cycles demonstrated that 35 cycles was in the linear range, thereby allowing comparison of abundance between brain regions.

Molecular cloning

Δ8b variants were cloned using overlapping extension PCR and KOD hot start DNA polymerase (Novagen, Madison, WI). Full-length cDNAs of the Δ8b variant were constructed by ligating an *Age*I (952)/*Bsm*BI (3642) fragment into a rat $Ca_v3.1a$ contained in pcDNA3 [7]. The sequence of this fragment was verified by automated sequencing at the University of Virginia Biomolecular Research Facility.

Overlap extension was also used to introduce the hemagluttinin epitope in the extracellular loop connecting IS5 and the pore loop (sequence added is underlined): TYNSSGRPQEHYPYDVPDYAVTFVDGRTSNTT. The epitope was subcloned into full-length WT and Δ8b by ligating an *Age*I (952)/*Hind*III (1577) and a *Hind*III (1577)/BsmBI (3642) fragment to *Age*I (952)/BsmBI (3642) digested $Ca_v3.1$ contained in pcDNA3.

Transfections

Human embryonic kidney 293 cells (HEK-293, CRL-1573, American Type Culture Collection, Manassas, VA) were grown in Dulbecco's modified medium F12 (DMEM/F-12 [Invitrogen]), supplemented with 10% fetal calf serum, penicillin G (100 units/ml), and streptomycin (0.1 mg/ml). Cells transiently expressed WT and Δ8b mutant of $Ca_v3.1$ channels using JET-PEI transfection reagents (PolyPlus, Illkirch, France). Cells for electrophysiology experiments were co-transfected with EGFP-expressing vector to identify transfected cells. Twenty-four to thirty-six hours post-transfection, the cells were dissociated by digestion with 0.25% trypsin plus 1 mM EDTA for two minutes, diluted 20-fold with DMEM, and then plated on glass cover slips. The cells were incubated at least four hours and up to 24 hours prior to electrophysiological studies. Each construct was tested in at least two transfections, and control data were collected from a number of transfections.

Electrophysiology

Whole cell Ca^{2+}-currents were recorded using the following external solution (in mM): 5 $CaCl_2$, 166 tetraethyl ammonium (TEA) chloride, and 10 HEPES, pH adjusted to 7.4 with TEA-OH. The internal pipette solution contained the following (in mM): 125 CsCl, 10 EGTA, 2 $CaCl_2$, 1 $MgCl_2$, 4 Mg-ATP, 0.3 Na_3GTP, and 10 HEPES, pH adjusted to 7.2 with CsOH. Currents were recording using an Axopatch 200B amplifier, computer (Dell, Round Rock, TX), Digidata 1322 A/D converter, and pCLAMP 9.0 software (Axon Instruments, Union City, CA). Unless otherwise noted, data were filtered at 2 kHz and digitized at 5 kHz. Recording pipettes were made from TW-150-6 capillary tubing (World Precision Instruments, Inc., Sarasota, FL), using a Model P-97 Flaming-Brown pipette puller (Sutter Instrument Co., Novato, CA). Once filled with the internal solution the pipette resistance was typically 2.4 MΩ. Only recordings with minimal leak currents were analyzed (<100 pA), therefore leak subtraction was not used. The average cell capacitance was ~10 pF. Series resistance was compensated between protocols to 70% (prediction and correction; 10 μs lag), resulting in maximal residual voltage error below 1.6 mV during measurement of the current-voltage (I–V) relationship. All experiments were performed at room temperature. Access resistance and cell capacitance were measured using on-line exponential fits to a capacitance transient (Membrane Test, Clampex). Access resistance averaged ~4 MΩ. Data from cells where the access resistance exceeded 5.5 MΩ were discarded. Activation and inactivation kinetics were calculated simultaneously using double exponential fits to the current trace using Clampfit 9.0 software (Axon Instruments). Steady-state activation and inactivation curves from each cell were fit in Excel using the Solver function, and then averaged.

We used the method of Agler et al., to estimate the probability of channel opening, P_o [8], which assumes no change in single channel current, reducing the relationship between whole cell current (I) to $I \approx NP_o$, where N is the number of channels in a cell and P_o is the probability of channel opening. N is estimated by measuring the channel gating current at the reversal potential for ionic current [8]. The area under this current represents the maximal gating charge Q_{max}, and is proportional to N. As described previously [9], peak ionic current conductance, G_{max}, was determined by fitting the *I–V* curve, obtained from the same cell, with a Boltzmann-Ohm equation. G_{max} is used as a proxy for *I* since it is not affected by changes in driving force. Therefore, the G_{max}/Q_{max} ratio can be used to estimate P_o [8].

Luminometry

HEK-293 cells were cultured in 24-well plates and transfected using JetPEI with 0.5 μg of DNA per well with the HA-tagged variants of $Ca_v3.1$, wt and Δ8b, as described earlier [4, 10]. The luminometric measurements were performed 48 h after transfection. Briefly, cells were rinsed and fixed for 5 min in 4% paraformaldehyde and then washed three times for 5 min with PBS. Half of the wells were permeabilized with 0.1% Triton X-100 for 5 min and rinsed three times with PBS. Cells were then incubated for 30 min in blocking solution (PBS plus 1% FBS). The HA–Ca_v3 proteins were detected using a monoclonal rat anti-HA antibody (1:1000, clone 3F10; Roche Diagnostics) after incubation for 1 hour at room temperature. After extensive washes (four times for 10 min in PBS plus 1% FBS), cells were incubated for 30 min with the secondary goat anti-rat antibody coupled to horseradish peroxidase (1:1000; Jackson ImmunoResearch, West Grove, PA). Cells were rinsed four times for 10 min with PBS before addition of SuperSignal enzyme-linked immunosorbent assay femto maximum sensitivity substrate (Pierce, Rockford, IL). The luminescence was measured using a Victor 2 luminometer (PerkinElmer, Wellesley, MA), and then protein amount in each well was measured with a BCA assay (Pierce) to normalize the measurements. The data were then normalized to the level of signal obtained for the wild-type (WT) HA–$Ca_v3.1$ protein in the non-permeabilized condition. Results are presented as mean ± s.e.m., and statistical differences were evaluated using Student's t-test.

Results

PCR of the region encoding the I–II loop detects splice variation

Total RNA was isolated from rat basilar artery, caudal cerebellar artery, and cerebral cortex, reverse transcribed into cDNA, and then PCR amplified. Multiple PCR products were amplified from each tissue (Fig. 1A). Sequencing demonstrated that the upper band (1270 bp) corresponded to the rat $Ca_v3.1a$, while the 868 bp band also corresponded to $Ca_v3.1$, but notably was missing 402 base pairs (GenBank accession numbers EF116284 and EF116283, respectively; [5]). Translation of this sequence revealed that the open reading frame was maintained (GenBank accession number ABL63738), suggesting that mRNA transcripts containing this deletion likely produce functional channels. Comparison of its nucleotide sequence to the rat genome (GenBank accession number NC_00519), indicated that the variant arises from an alternative acceptor site in the middle of exon 8 (exon 8 begins at IS6), therefore we refer to the deletion variant as Δ8b (Fig. 1B). The 816 bp band corresponded to a variant that contained both the 402 bp deletion and a second 51 bp deletion that leads to the loss of 17 amino acids that encode IS6 (Genbank accession number FJ227500). Detection of this variant was variable amongst juvenile rat brain preparations and negligible in adult rat brain (Fig. 1A and B, respectively). It is unlikely that the 816 bp variant would encode a functional channel as S6 segments form the channel wall, and the hydrophobic residues of IS6 are replaced by highly-charged amino acids, and therefore, was not studied further. Expression of the Δ8b variant was detected in all rat brain regions tested (Fig. 1C). Densitometry analysis indicated that the Δ8b variant was more abundant than WT $Ca_v3.1$ in medulla, spinal cord, and pineal gland, and less abundant in basilar artery, caudal cerebellar artery, and pituitary (Fig. 1D). Previous studies on the I–II loop in related human Ca_v3 channels [4,6], uncovered two roles of this loop: one, it modulates channel gating; and two, it controls surface expression. For example, a D3-5 deletion that covers a similar region of the loop (Fig. 1B) was found to increase surface expression over 5-fold in human $Ca_v3.2$ [4], while increasing surface expression for the human $Ca_v3.1$ by only 1.5-fold over WT channels [6]. In the light of these data, we have therefore analyzed the functional consequence -gating and surface expression - of this naturally occurring Δ8b splice variation of the I–II loop of rat $Ca_v3.1$.

$Ca_v3.1$_Δ8b deletion reveals no shift in the voltage-dependence of channel gating

Full-length versions of $Ca_v3.1$ containing either the full exon 8 sequence or the Δ8b deletion were constructed in a mammalian expression vector. These plasmids were then transiently-transfected into HEK-293 cells, and the resulting channels were studied using whole cell patch clamp electrophysiology. Robust currents were readily detected using 5 mM Ca^{2+} as charge carrier (1.5–2.5 nA). The activation and inactivation kinetics of WT and Δ8b currents were not significantly different (Fig. 2A, Table 1). The voltage dependence of activation was measured using a standard current-voltage (*I–V*) protocol with 5 mV steps to varying potentials from a holding potential of −100 mV. Normalized peak current relationships for WT and Δ8b channels were indistinguishable (Fig. 2B, Table 1). The voltage dependence of inactivation was measured using 15 s prepulses to varying potentials, followed by a test pulse to −20 mV to measure channel availability. Representative current traces obtained during the test pulse are shown in Fig. 2C. Average data clearly show that the Δ8b deletion did not affect steady-state inactivation (Fig. 2D, Table 1).

$Ca_v3.1$_Δ8b channels show higher expression at the plasma membrane

Peak Ca^{2+} current density was significantly higher for the Δ8b variant than WT channels. To rule out any changes in driving force, we calculated the chord conductance of the current and normalized this to cell size as judged by cell capacitance (Fig. 3A). This analysis revealed a 1.8-fold increase in Ä8b channel density relative to WT channels.

An independent method to measure surface expression of proteins is to use antibodies directed against extracellular epitopes, and then measure expression at the surface under non-permeabilized conditions (Fig. 3B) and total expression after Triton X-100 permeabilization (Fig. 3C). Using this method we previously demonstrated that deletions in the I–II loop lead to large increases in the surface expression of $Ca_v3.2$ [4], as well as significant increase in human $Ca_v3.1$ surface expression [6]. To apply this method to rat $Ca_v3.1$, we engineered a hemagluttinin (HA) tag in the extracellular loop connecting IS5 to the pore loop (see Methods for details). Electrophysiological testing of the tagged channel revealed no change in channel gating (example trace shown in Fig. 2A). To measure surface expression, transfected cells were treated with an anti-HA monoclonal antibody followed by a secondary antibody coupled to horseradish peroxidase and SuperSignal substrate. Luminometry analysis revealed a significant 1.3-fold in surface expression of Ä8b channel relative to WT channels (Fig. 3B) with no effect on its total expression (Fig. 3C), indicating that the Δ8b deletion of the I–II loop of $Ca_v3.1$ exert its predominant effect on the expression of the channel protein at the plasma membrane (Fig. 3D).

In addition to increase in Ca^{2+} current density, as well as increase in channel protein at the plasma membrane, evidence for higher probability of channel opening (P_o) were found with some I–II loop deletion mutants of Ca_v3 channels [6]. To test for this possibility, we used the G_{max}/Q_{max} method to estimate channel P_o [8]. The protocol used to elicit gating currents and representative traces are shown in Fig. 4A. Linear regression analysis of plots of the G_{max}/Q_{max} ratio for WT and Δ8b channels revealed a similar slope, indicating that channel P_o was not affected (Fig. 4B). Taken together the electrophysiology and luminometry studies clearly show that the Δ8b deletion increases T-currents by increasing the expression of $Ca_v3.1$ channels at the plasma membrane.

Discussion

A key finding of this study was the existence of a novel $Ca_v3.1$ splice variant whose abundance is differentially regulated in various brain regions. This indicates both the importance of the Δ8b variant and that splicing of exon 8 is regulated. A second key finding was that this variation

increased expression of functional channels at the plasma membrane. This result is significant because increased T-current density is thought to underlie neurological disorders characterized by thalamocortical dysrhythmia [11], such as absence epilepsy [12].

$Ca_v3.1$ channels are encoded by the *CACNA1G* gene. The splicing of this gene in humans has been studied extensively [13–15]. Splice variation alters the sequence of the II–III loop, the III–IV loop, and the carboxy terminus, leading to the production of at least 30 distinct transcripts [15]. The most common transcript is the $Ca_v3.1$ "a" isoform, which together with the Δ14 variant account for 71% of all transcripts [15]. Splice variation has been shown to alter the biophysical properties of $Ca_v3.1$ channels, shifting both the voltage dependence and kinetics [14,15]. Although the Δ8b variant did not alter channel gating, this is the first study to discover that splice variation modifies trafficking of $Ca_v3.1$ channels. We hypothesize that the region encoded by exon 8 contains motifs that are recognized by proteins that control movement of proteins to and/or from the plasma membrane. For example, the loop contains the MxxxL motif that mediates internalization of proteins such as prostate-specific membrane antigen [16]. A limitation to these studies is that splice variation has only been detected at the mRNA transcript level due to the lack of variant specific antibodies.

$Ca_v3.1$ mRNA, T-currents, and $Ca_v3.1$ protein are distributed throughout the brain and cardiovascular system (reviewed in [17]). Distribution of its mRNA in rat brain was mapped in fine detail by Talley et al. [18]. Notably it was abundantly expressed in thalamic relay nuclei, a brain region where T-channel mediated low threshold spikes have been studied extensively. Studies of knockout mice confirmed $Ca_v3.1$ is the only T-channel expressed in thalamic relay nuclei, and without this current, mice are less susceptible to agents that cause absence seizure-like activity [19]. Modeling studies of thalamocortical neurons predict that changes in T-current density, as observed in this study, would increase rhythmic spike generation [20]. Upregulation of thalamic T-currents is thought to play a key role in triggering absence epilepsy seizures in animals [12]. Notably, this occurs without any change in $Ca_v3.1$ mRNA levels [12]. Our finding that splice variation alters surface expression provides a possible explanation for this result: a switch in $Ca_v3.1$ splicing to the Δ8b isoform would increase T-currents and rhythmic firing, and contribute to seizure susceptibility [21].

The I–II loop of high voltage-gated Ca^{2+} channels is a major locus for their control by auxiliary subunits and second messenger cascades [22]. The analogous loop in low voltage-activated, $Ca_v3.2$ channels, also plays critical roles in controlling channel gating and expression [4]. Notably, mutations found in childhood absence epilepsy patients alter these properties in a manner that would increase neuronal excitability, and thereby contribute to seizure susceptibility [23]. Our studies provide the basis to predict that mutations and/or splicing in the I–II loop of $Ca_v3.1$ might increase T-channel expression, and if so would contribute to a wide range of disorders characterized by thalamocortical dysrhythmia [11]. In addition, T-currents in some, but not all, thalamic relay nuclei are regulated by an ATP-dependent phosphorylation mechanism [24]. It is tempting to speculate that splice variation such as that described in this study would be responsible for this regional heterogeneity. Notably, the region deleted in Δ8b channels contains many consensus motifs for phosphorylation by protein kinase A, C, and CaMKII. Notably, $Ca_v3.1$ currents are upregulated in a PKA- and temperature-dependent manner and the phosphorylation site responsible for this effect is unknown [25].

In conclusion, the present study establishes that splice variation of the I–II linker region of $Ca_v3.1$ alters the trafficking of channels to the plasma membrane, resulting in increased surface expression. In contrast, no effect on the voltage dependent gating of these channels was found, suggesting that expression of this novel splice variant is not responsible for the higher voltage activation reported previously in the basilar artery [5]. Nevertheless, the increased surface expression and current density afforded by the variant could point to a more dominant role for

Ca_v3 channels in arterial excitability, as occurs in neurons. Surprisingly little is known about the mechanisms that control trafficking of Ca_v3 proteins to the cell membrane. Consideration of alternative splicing as a mechanism capable of impacting on surface expression of T channels is novel and will merit further interest with respect to normal physiology (development, aging) and disease states in which T-current density is known to vary significantly.

Acknowledgments

This work was supported by the following: a National Institute of Health Grant NS038691 (to E.P.R.), an Epilepsy Foundation Predoctoral Fellowship (to J.P.B.), a Sigma Xi Grant-in-Aid of Research (to J.P.B.), a La Ligue Française contre l'Epilepsie fellowship (to I.B.), a Agence Nationale pour la Recherche grant 06-NEURO-035-01 (to P.L.), a Fondation pour la Recherche sur le Cerveau (to P.L.), and a National Health and Medical Research Council of Australia grant 471420 (to C.E.H.).

References

1. Perez-Reyes E, Lory P. Molecular biology of T-type calcium channels. CNS Neurol Disord Drug Targets 2006;5:605–609. [PubMed: 17168745]
2. Arias JM, Murbartián J, Vitko I, Lee JH, Perez-Reyes E. Transfer of β subunit regulation from high to low voltage-gated Ca^{2+} channels. FEBS Letters 2005;579:3907–3912. [PubMed: 15987636]
3. Li JY, Stevens L, Wray D. Molecular regions underlying the activation of low- and high-voltage activating calcium channels. European Biophysics Journal with Biophysics Letters 2005;34:1017–1029. [PubMed: 15924245]
4. Vitko I, Bidaud I, Arias JM, Mezghrani A, Lory P, Perez-Reyes E. The I–II loop controls plasma membrane expression and gating of $Ca_v3.2$ T-type Ca^{2+} channels: a paradigm for Childhood Absence Epilepsy. Journal of Neuroscience 2007;27:322–330. [PubMed: 17215393]
5. Navarro-Gonzalez MF, Grayson TH, Meaney KR, Cribbs LL, Hill CE. Non L-type voltage dependent calcium channels control vascular tone of the rat basilar artery. Clin Exp Pharmacol Physiol. 2008
6. Baumgart JP, Vitko I, Bidaud I, Kondratskyi A, Lory P, Perez-Reyes E. I–II loop structural determinants in the gating and surface expression of low voltage-activated calcium channels. PLoS ONE 2008;3:e2976. [PubMed: 18714336]
7. Perez-Reyes E, et al. Molecular characterization of a neuronal low-voltage-activated T-type calcium channel. Nature 1998;391:896–900. [PubMed: 9495342]
8. Agler HL, Evans J, Tay LH, Anderson MJ, Colecraft HM, Yue DT. G protein-gated inhibitory module of N-type ($Ca_v2.2$) Ca^{2+} channels. Neuron 2005;46:891–904. [PubMed: 15953418]
9. Arias-Olguín II, et al. Characterization of the gating brake in the I–II loop of $Ca_v3.2$ T-type Ca^{2+} channels. J. Biol. Chem 2008;283:8136–8144. [PubMed: 18218623]
10. Dubel SJ, Altier C, Chaumont S, Lory P, Bourinet E, Nargeot J. Plasma membrane expression of T-type calcium channel α1 subunits is modulated by HVA auxiliary subunits. J. Biol. Chem 2004;279:29263–29269. [PubMed: 15123697]
11. Llinás RR, Ribary U, Jeanmonod D, Kronberg E, Mitra PP. Thalamocortical dysrhythmia: A neurological and neuropsychiatric syndrome characterized by magnetoencephalography. Proc Natl Acad Sci U S A 1999;96:15222–15227. [PubMed: 10611366]
12. Zhang Y, Mori M, Burgess DL, Noebels JL. Mutations in high-voltage-activated calcium channel genes stimulate low-voltage-activated currents in mouse thalamic relay neurons. J. Neurosci 2002;22:6362–6371. [PubMed: 12151514]
13. Mittman S, Guo J, Agnew WS. Structure and alternative splicing of the gene encoding α1G, a human brain T calcium channel α1 subunit. Neurosci Lett 1999;274:143–146. [PubMed: 10548410]
14. Chemin J, Monteil A, Bourinet E, Nargeot J, Lory P. Alternatively spliced α1G ($Ca_v3.1$) intracellular loops promote specific T-type Ca^{2+} channel gating properties. Biophys J 2001;80:1238–1250. [PubMed: 11222288]
15. Emerick MC, Stein R, Kunze R, McNulty MM, Regan MR, Hanck DA, Agnew WS. Profiling the array of $Ca_v3.1$ variants from the human T-type calcium channel gene CACNA1G: Alternative structures, developmental expression, and biophysical variations. Proteins-Structure Function and Bioinformatics 2006;64:320–342.

16. Rajasekaran SA, Anilkumar G, Oshima E, Bowie JU, Liu H, Heston W, Bander NH, Rajasekaran AK. A novel cytoplasmic tail MXXXL motif mediates the internalization of prostate-specific membrane antigen. Mol Biol Cell 2003;14:4835–4845. [PubMed: 14528023]

17. Perez-Reyes E. Molecular physiology of low-voltage-activated T-type calcium channels. Physiol Rev 2003;83:117–161. [PubMed: 12506128]

18. Talley EM, Cribbs LL, Lee JH, Daud A, Perez-Reyes E, Bayliss DA. Differential distribution of three members of a gene family encoding low voltage-activated (T-type) calcium channels. J Neurosci 1999;19:1895–1911. [PubMed: 10066243]

19. Kim D, Song I, Keum S, Lee T, Jeong MJ, Kim SS, McEnery MW, Shin HS. Lack of the burst firing of thalamocortical relay neurons and resistance to absence seizures in mice lacking α1G T-type Ca^{2+} channels. Neuron 2001;31:35–45. [PubMed: 11498049]

20. McCormick DA, Huguenard JR. A model of the electrophysiological properties of thalamocortical relay neurons. J Neurophysiol 1992;68:1384–1400. [PubMed: 1331356]

21. Chorev E, Manor Y, Yarom Y. Density is destiny--on the relation between quantity of T-type Ca^{2+} channels and neuronal electrical behavior. CNS Neurol Disord Drug Targets 2006;5:655–662. [PubMed: 17168749]

22. Richards MW, Butcher AJ, Dolphin AC. Ca^{2+} channel β-subunits: structural insights AID our understanding. Trends Pharmacol Sci 2004;25:626–632. [PubMed: 15530640]

23. Vitko I, Chen Y, Arias JM, Shen Y, Wu XR, Perez-Reyes E. Functional characterization and neuronal modeling of the effects of Childhood Absence Epilepsy variants of *CACNA1H*, a T-type calcium channel. J Neurosci 2005;25:4844–4855. [PubMed: 15888660]

24. Leresche N, Hering J, Lambert RC. Paradoxical potentiation of neuronal T-type Ca^{2+} current by ATP at resting membrane potential. J. Neurosci 2004;24:5592–5602. [PubMed: 15201332]

25. Chemin J, Mezghrani A, Bidaud I, Dupasquier S, Marger F, Barrere C, Nargeot J, Lory P. Temperature-dependent modulation of Ca_V3 T-type calcium channels by protein kinases C and A in mammalian cells. J. Biol. Chem 2007;282:32710–32718. [PubMed: 17855364]

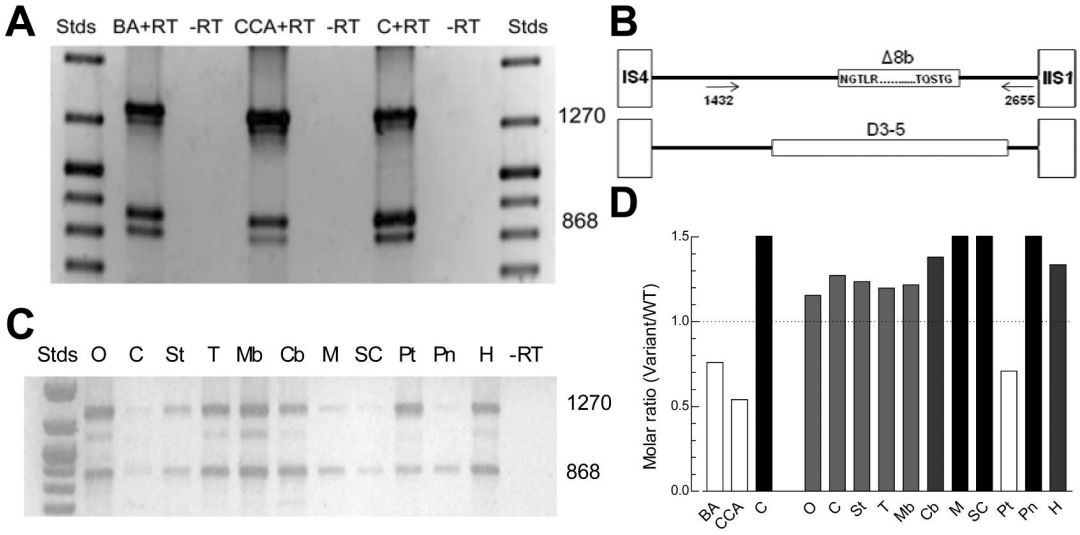

Fig. 1. PCR of I–II linker splice variants of $Ca_v3.1$

A, PCR results obtained using juvenile basilar artery, caudal cerebellar artery, and cerebral cortex. Strong bands of 1270 and 868 bp were found in each tissue. Stds, MW markers; BA, basilar artery; CCA, caudal cerebellar artery; C, cortex; +RT, RNA with reverse transcriptase: −RT, RNA without reverse transcriptase. **B**, Schematic showing the location of Exon 8 in the loop connecting IS6 to IIS1, and the PCR primers. For comparison, the D3-5 region previously deleted in human $Ca_v3.1$ and $Ca_v3.2$ is shown below [4,6]. **C**, PCR results obtained using various rat brain regions: O, Olfactory bulb; C, cortex; St, striatum; T, thalamus/diencephalon; Mb, midbrain; Cb, cerebellum; M, medulla; SC, spinal cord; Pt, pituitary; Pn, pineal; and H, hippocampus. **D,** Abundance of the Δ8 variant relative to wild-type $Ca_v3.1$. Results are from the representative experiments shown in panels A (N=5) and B (n=3)

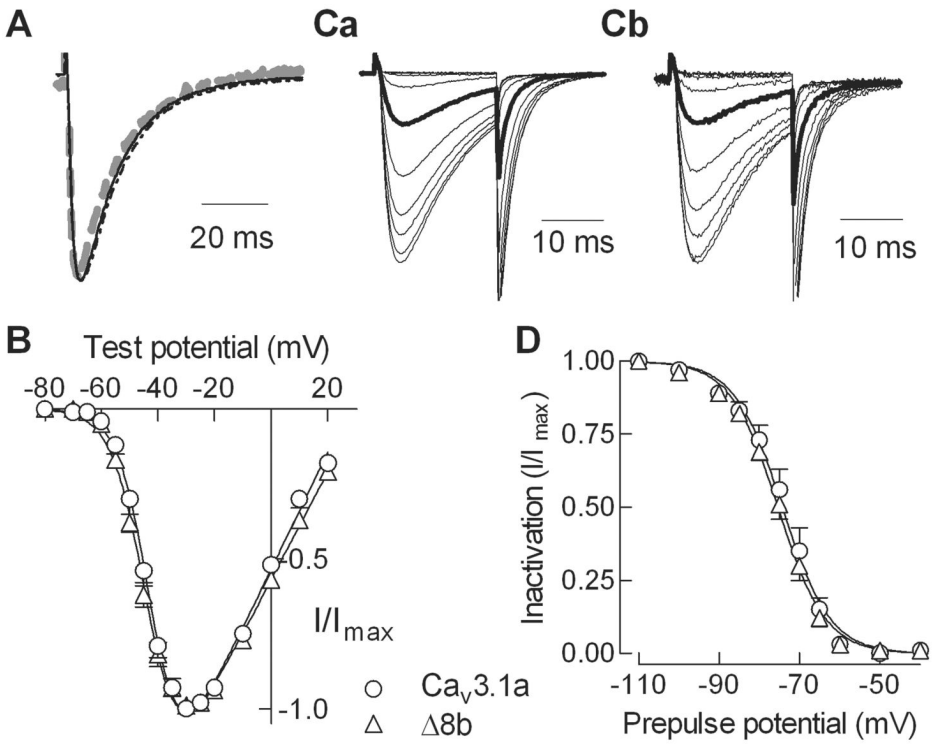

Fig. 2. Electrophysiological properties of WT and Δ8b splice variant of rat $Ca_v3.1$

A, Normalized current traces obtained during a step depolarization to −20 mV from a holding potential of −100 mV. Cells were transiently transfected with cDNAs encoding either WT (solid line), Δ8b (dotted line), or HA-tagged WT channels (dotted gray line). **B**, Normalized peak current-voltage relationships for WT and Δ8b channels. Data from individual cells was normalized to the maximum current in each cell, and then averaged. Smooth lines represent fit to the average data using a Boltzmann-Ohm function [9]. The data from each cell were also fit with this equation, and the V_{50} values were averaged (Table 1). **C**, Normalized current traces obtained during steady-state inactivation protocol. The duration of the prepulse used to inactivate channels was 15 s. Data for WT channels is shown in panel Ca, and for Δ8b in panel Cb. Data obtained after a prepulse to −75 mV is shown in bold. **D**, Average steady-state inactivation curves for both variants. As for the I–V graph, data represent average ± s.e.m. and the smooth curve represents a fit using a Boltzmann equation [9] (results in Table 1).

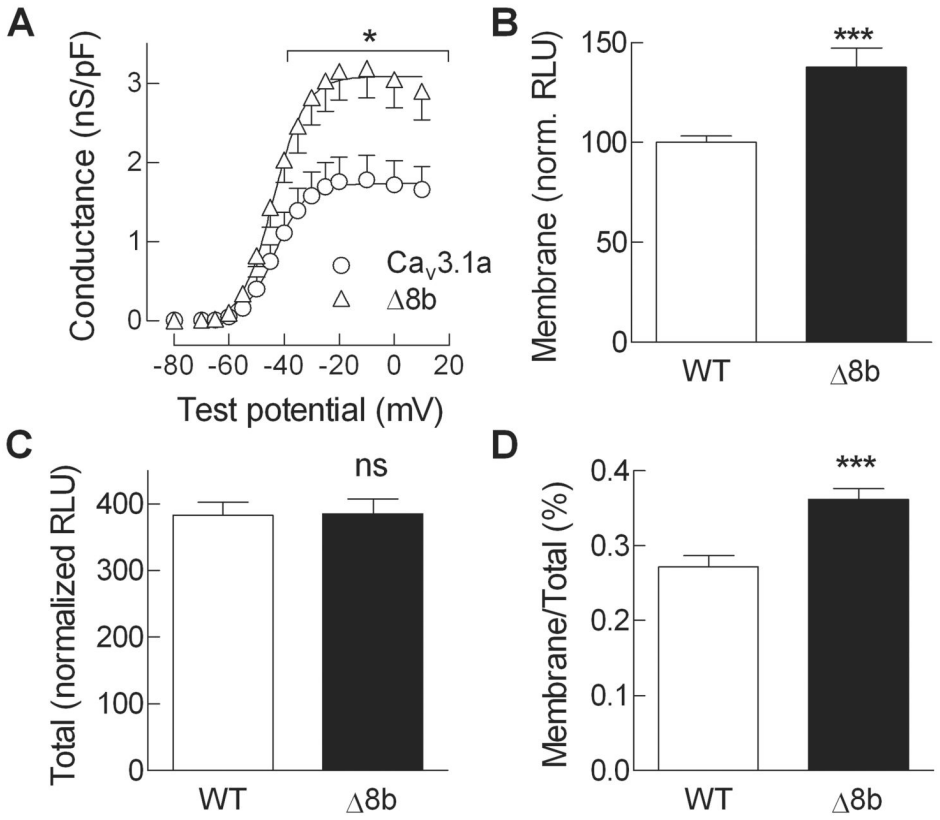

Fig. 3. Surface expression of WT and Δ8b channels as assessed by electrophysiology and luminometry

A, Peak whole cell Ca^{2+} currents were fit with the Boltzmann-Ohm equation to calculate V_{50}, k, G_{max}, and V_{rev}. The V_{rev} value was then used to calculate a chord conductance for the peak ionic current in each cell. Data shown are average ± s.e.m. of 8–12 cells. Statistically different ($P<0.05$) data points are indicated with an asterisk. **B**, Surface expression of HA-tagged WT and Δ8b protein as assessed by a luminometry method [10]. Channel protein at the plasma membrane (Membrane) was measured in non-permeabilized condition, and expressed as percent signal detected with WT channels (approximately 3×10^6 relative light units). **C**, Total surface expression measured after permeabilization with Triton X-100, also expressed as percent of WT control observed under non-permeabilized condition. **D**, The ratio of the Membrane signal divided by the Total signal yields the percent of channels that are at the plasma membrane. Data represent average of 19–24 experiments. The increased surface expression of Δ8b was highly significant ($P<0.001$).

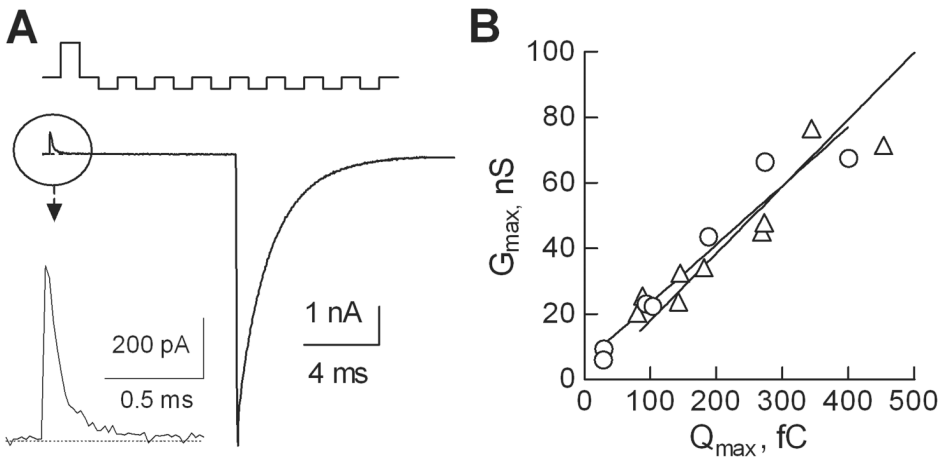

Fig. 4. The effect of splice variation on the probability of channel opening as assessed using the gating charge method

Maximal gating charge was measured at the reversal potential using a P/−8 protocol to cancel capacitative transients (A, top). A representative current trace recorded during the step depolarization to +50 mV (average of 10 consecutive sweeps) is shown in two scales. **B**, Correlation between the gating current (Q_{max}) and maximal conductance (G_{max}) for WT and Δ8b channels (same symbols as in panel A). Linear regression analysis indicates that the slopes, which are proportional to $P_{o,max}$, are not statistically different (~0.2 nS/fC, P<0.4).

Table 1

Electrophysiological properties of $Ca_v3.1a$ and $Ca_v3.1\Delta8$

	Density	Activation		Inactivation			Kinetics at −20 mV		
	G_{max} (nS/pF)	V_{50} (mV)	k (mV)	V_{50} (mV)	k (mV)	n	τ act (ms)	τ inact (ms)	n
$Ca_v3.1a$	1.8 ± 0.3	−42.1 ± 1.1	5.3 ± 0.2	−74.1 ± 1.6	−5.3 ± 0.2	7	1.6 ± 0.2	13.9 ± 1.1	8
$Ca_v3.1\Delta8b$	3.2 ± 0.4*	−43.5 ± 0.9	5.5 ± 0.2	−75.2 ± 1.0	−5.5 ± 0.2	11	1.7 ± 0.2	13.4 ± 0.5	12

Statistical significance was determined using Student's t-test. An asterisk denotes where < 0.05. The G_{max}, V_{50} of activation, and kinetic parameters were all determined from the *I–V* protocol, and therefore have the same number of cells in each measurement.